

Observation of magnetization surface textures of the van der Waals antiferromagnet FePS₃ by spin Hall magnetoresistance

F. Feringa,^{1,*} G. E. W. Bauer,^{1,2} and B. J. van Wees^{1,†}

¹*Physics of Nanodevices, Zernike Institute for Advanced Materials, University of Groningen, 9747 AG Groningen, The Netherlands*

²*AIMR & Institute for Materials Research, Tohoku University, Aoba-ku, Katahira 2-1-1, Sendai, Japan*

Van der Waals materials are a new platform to study two-dimensional systems, including magnetic order. Since the number of spins is relatively small, measuring the magnetization is challenging. Here we report spin Hall magnetoresistance (SMR) up to room temperature caused by the magnetic surface texture of exfoliated flakes of magnetic van der Waals materials. For the antiferromagnet FePS₃ the SMR amounts to 0.1 % for an applied magnetic field of 7 T at 5 K which implies a substantial canting of the magnetic moments relative to the colinear antiferromagnetic order. The canting is substantial even for a magnetic field along the Néel vector, which illustrates the unique power of the SMR to detect magnetic surface textures in van der Waals magnets.

The magnetic susceptibility is a crucial material property that can be measured by many techniques, such as vibrating sample, torque, or squid magnetometry [1]. Since signals are proportional to the total magnetization, these techniques are not sensitive to the relatively small number of spins at the surface of bulk crystals or in two-dimensional van der Waals materials.

The spin Hall magnetoresistance (SMR) in heavy metal contacts to (preferably electrically insulating) ferromagnets senses only the spin configuration at the interface and is therefore well suited to study the magnetic properties of the surfaces of bulk magnets or van der Waals (vdW) magnets [2, 3] down to monolayer thicknesses. The SMR is governed by the exchange interaction $\sim \vec{\sigma} \cdot \vec{m}$ of the spins of conduction electrons with polarization $\vec{\sigma}$ in the heavy metal and the local moment direction \vec{m} in the magnet [4–7]. The resistance of Pt contacts to ferromagnetic insulators is lowest when $\vec{\sigma} \parallel \vec{m}$ by combination of the direct and inverse spin Hall effects. In antiferromagnets the SMR may become “negative”, i.e. a minimum resistance when the Néel vector is parallel to $\vec{\sigma}$ ($\vec{\sigma} \parallel \vec{n}$); note that in the absence of in-plane anisotropy the Néel vector orients normal to the applied magnetic field due to the minimization of the exchange and Zeeman energy [8, 9]. SMR has been observed in paramagnetic CoCr₂O₄ [10], amorphous YIG [11], Cr₂O₃ [12], NdGaO₃ [13], and gadolinium gallium garnet (GGG) [14]. The SMR revealed magnetic phase transitions in α -Fe₂O₃ [15], CoCr₂O₄ [10], and DyFeO₃ [16] and magnetic domain structures [17].

The SMR in the longitudinal resistance of a metal contact on an antiferromagnet with two sublattices *A* and *B* reads

$$\text{SMR} = \rho_L - \rho_0 = \frac{1}{2} \sum_{X=A,B} \rho_1^{(X)} \left[1 - (\vec{m}^{(X)} \cdot \vec{\sigma})^2 \right] \quad (1)$$

where $\rho_1^{(X)}$ is the SMR coefficient for the sublattice *X* with local moment magnetization $\vec{m}^{(X)}$ controlled by an

applied magnetic field, while $\vec{\sigma}$ is the current-induced spin accumulation direction generated by the spin Hall effect in the current-biased contact [9, 19].

Here we report for the first time observation of an SMR on the exfoliated van der Waals material FePS₃, an uniaxial antiferromagnet with perpendicular magnetic anisotropy. The SMR persists above the Néel temperature in the paramagnetic regime up to 300 kelvin. We

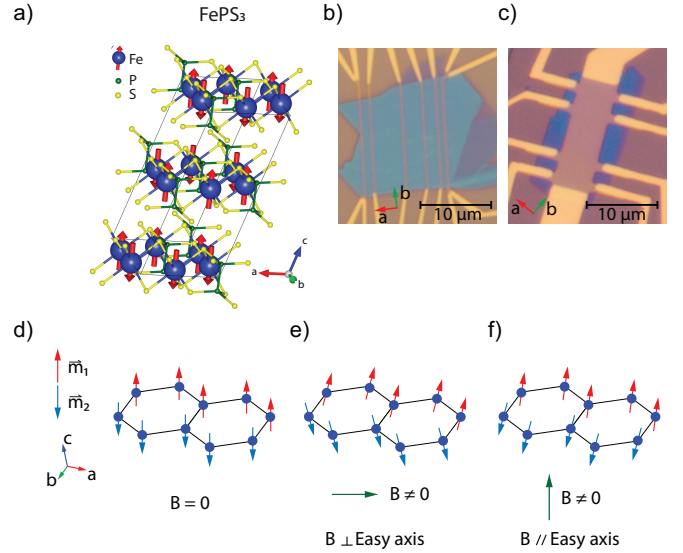


FIG. 1. a) Crystal structure of FePS₃ generated by VESTA [18]. The red arrows are the directions of the Fe²⁺ magnetic moments at zero magnetic field with the easy axis normal to the **a-b** crystal plane. b) and c) are the experimental samples imaged by optical microscopy. d-f) Schematic response of the magnetic sublattices *m*⁽¹⁾ and *m*⁽²⁾ without and with magnetic field parallel and perpendicular to the **a-b** plane, respectively. A magnetic field along **a**, normal to the easy axis, generates a transverse magnetization, while a magnetic field along the easy axis causes an unconventional canting also in the **a** direction.

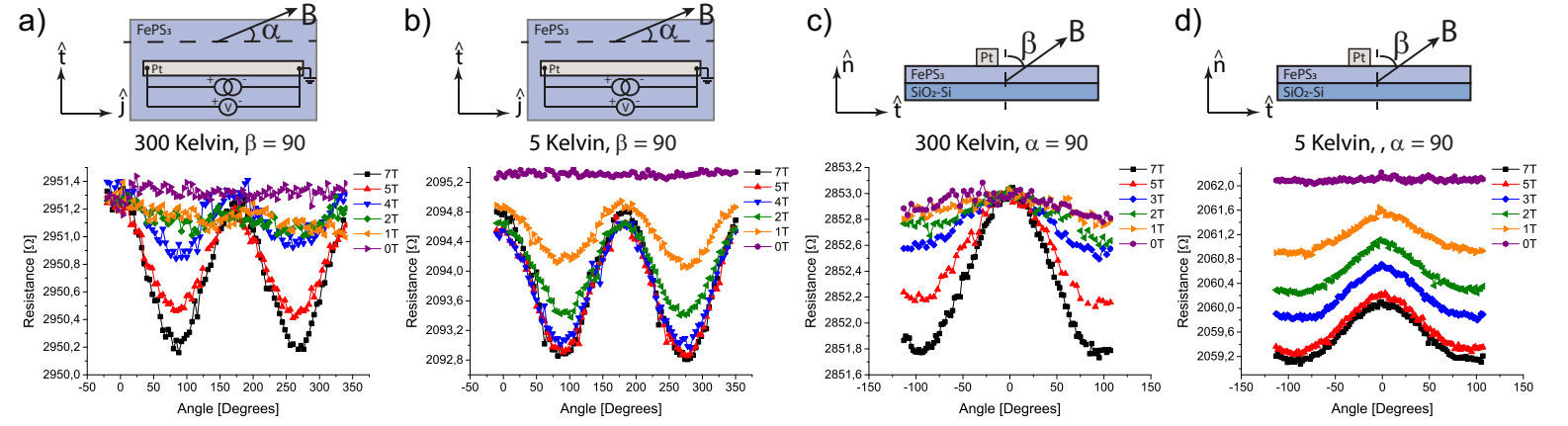


FIG. 2. SMR response for an in-plane and out-of-plane rotation of an external magnetic field at 300 and 5 Kelvin at various magnetic field strengths. The decrease of the background resistance at 5 kelvin between 0 and 1 tesla in b) and d) is attributed to suppression of weak localization effects in Pt.

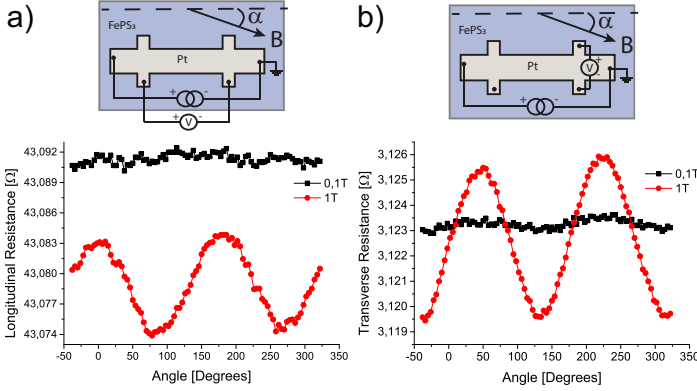


FIG. 3. The a) longitudinal and b) transverse response to a rotating magnetic field of 0.1 and 1 Tesla for a current density of $11 \times 10^{-14} \text{ A/m}^2$ at 10 kelvin. The sign corresponds to a positive SMR and the ratio of the amplitudes agrees with the aspect ratio of 1.6 of the Hall bar. The decrease of the background resistance between 0.1 and 1 tesla is attributed to suppression of weak localization effects in Pt, similar to what is observed in Fig. 2.

discover an unusual symmetry breaking of the surface magnetic textures by out-of-plane magnetic fields that cannot be accessed by conventional magnetometry.

FePS₃ is a transition metal phosphorus trichalcogenide MPX₃, where M is a transition metal and X is a chalcogenide, which all crystallize with monoclinic space group C_2^2/m symmetry [21]. MnPS₃ and FePS₃ are uniaxial antiferromagnets, while NiPS₃ is an easy-plane antiferromagnet. Below the Néel temperature $T_N = 120 \text{ K}$ [22] two nearest neighbor moments in a FePS₃ layer order ferromagnetically and one nearest neighbor antiferromagnetically. Neighboring layers in turn order antiferromagnetically [23], as shown in Fig. 1a). The bandgap of FePS₃ is 1.5 eV [24] and we find that FePS₃ effectively behaves as a good electric insulator [25].

We mechanically exfoliated FePS₃ on a SiO₂-Si substrate and in a nitrogen atmosphere by adhesive tapes [26] from a bulk crystal [27]. We patterned Hall bars and strips on top of 20 nm and 40 nm thick FePS₃ flakes by conventional electron beam lithography, followed by dc sputtering deposition of $\approx 7 \text{ nm}$ of Pt. The Pt strips (Hall bar) are 400 nm (5 μm) wide and approximately 15 μm (15 μm) long. Ti-Au (5-55nm) leads deposited by e-beam evaporation connect the Pt Hall bar and strips to a chip carrier by AlSi wires. Fig. 1b) and c) shows images of the experimental samples.

We applied AC currents $I_{rms} = 100 \mu\text{A} - 4 \text{ mA}$ at $\omega = 8 \text{ Hz}$ to the Pt strips and Hall bar and measured the voltages over the longitudinal and transverse directions. The current generates a spin accumulation at the interface that interacts with the surface magnetization. The associated Joule heating generates a temperature gradient in the magnet via the bulk spin Seebeck effect (SSE) that scales quadratically with the current. Lock-in amplifiers separately measure the first $R_{1\omega} = V_{1\omega}/I$ and second $R_{2\omega} = V_{2\omega}/I^2$ harmonic response. We also monitor the conduction of FePS₃ between two Pt strips, thereby excluding parasitic current flow through FePS₃, as shown in the supplementary material (SM) Fig. S3.

Here we focus on $R_{1\omega}$, i.e. the SMR as a function of external magnetic field at in-plane and out-of-plane angles relative to the Pt contact as summarized in Fig. 2 for the strip and Fig. 3 for the Hall bar device. The field generates a net magnetization in the antiferromagnet by canting the local moments, as shown in Fig. 1e). Since the in-plane magnetic anisotropy is small, the in-plane magnetization closely follows the magnetic field direction. When rotating a field with constant strength from the hard in-plane to an easy normal direction, the in-plane magnetization must decrease. Up to an applied magnetic field of $|\vec{B}| = 7 \text{ T}$, we do not observe a magnetic

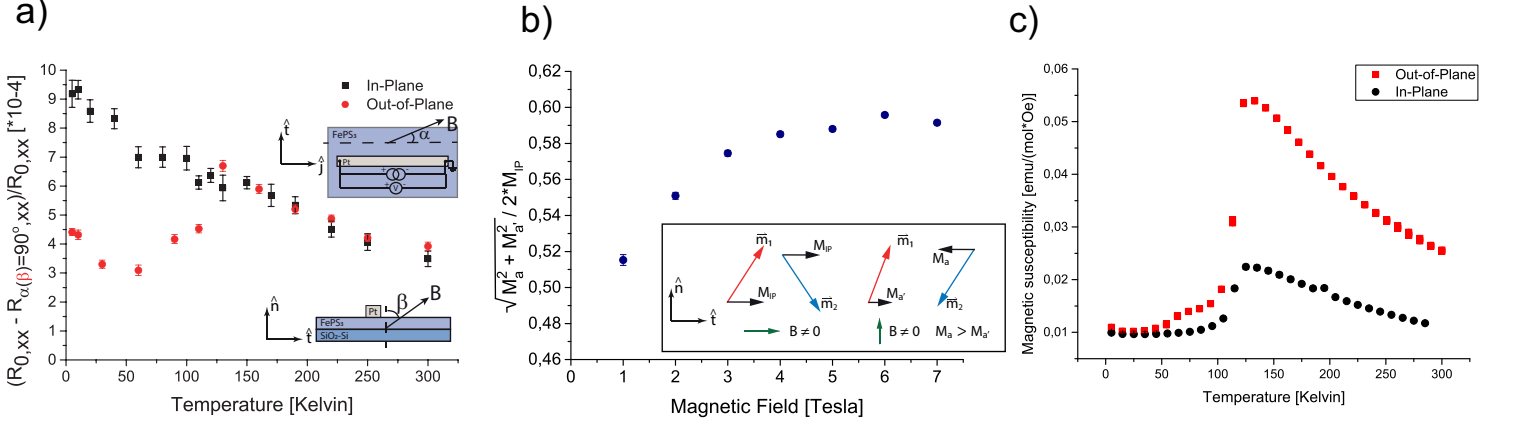


FIG. 4. a) SMR signals as a function of temperature for an in-plane and out-of-plane rotation of the magnetic field with $\alpha = \beta = 90^\circ$ and $B = 7$ T. b) Ratio $\sqrt{M_a^2 + M_{a'}^2}/2M_{IP}$ for various magnetic field strengths at $T = 5$ K extracted by fitting Eq. (3) to Fig. 2d). Inset shows the definitions of M_{IP} , $M_{a'}$ and M_a . c) The magnetic susceptibilities of bulk FePS₃ for in-plane and out-of-plane magnetic fields. See [20] for more details.

(such as a spin-flop) phase transition or saturation of the in-plane magnetization, consistent with [28]. Fig. 3a) and b) display the transverse and longitudinal response measured in the Hall bar. The observed “positive” SMR in Pt on FePS₃ is similar to that of ferromagnets and a consequence of the strong out-of-plane anisotropy. Due to the out-of-plane sub lattice magnetization, the spin absorption is maximum for $\vec{B} = 0$, resulting in $\vec{m}^{(X)} \cdot \vec{\sigma} = 0$ and therefore a higher Pt resistance. An in-plane magnetic field generates an in-plane magnetization parallel to the magnetic field $\vec{m}^{(X)} \parallel \vec{B}$ as shown in Fig. 1e). As a consequence, the spin absorption is reduced, which lowers the Pt resistance when the applied magnetic field is parallel to the spin accumulation ($\vec{B} \parallel \vec{\sigma}$), resulting in a “positive” SMR for fields up to 7 T.

Figure 4a) shows the SMR at various temperatures for an in-plane and out-of-plane magnetic field of $|\vec{B}| = 7$ T. The SMR measured in the out-of-plane rotation of the magnetic field displays a pronounced cusp at T_N , very similar to the separately measured out-of-plane magnetic susceptibility in Fig. 4c), which is typical for an antiferromagnetic phase transition. On the other hand, the in-plane SMR increases monotonically with decreasing temperature. The in-plane magnetic susceptibility in Fig. 4c) has a step at T_N , but this feature is much weaker than the step in the out-of-plane susceptibility.

A spin model, which only includes uniaxial anisotropy, exchange, and Zeeman interaction, cannot describe the difference between the observed in-plane and out-of-plane rotations below T_N because the spin absorption should be maximum when the magnetic field is perpendicular to the spin accumulation (for $\alpha = 0^\circ$ and $\beta = 0^\circ$), i.e. $\vec{m}^{(X)} \cdot \vec{\sigma} = 0$ for $\vec{B} \cdot \vec{\sigma} = 0$. Moreover, Fig. 2d) reveals an unexpected decrease of the entire angle-dependent out-of-plane SMR at low temperatures.

The observations indicate that both sublattices 1 and 2, originally parallel and antiparallel to an out-of-plane magnetic field, cant into the crystallographic **a** direction as sketched in Fig. 1f) and in the inset of Fig. 4b). Since the canting occurs by a gain in the Zeeman energy, the canting angle of sublattice 2 must be larger than that of $X = 1$. For $\alpha = 90^\circ$ we may interpolate the projections of the sublattice magnetizations $m^{(X)}(B, \beta) = \vec{m}^{(X)} \cdot \vec{\sigma}$ as

$$m^{(1)}(B, \beta) = M_{IP}(B) \sin \beta + M_a(B) \cos \beta \quad (2a)$$

$$m^{(2)}(B, \beta) = M_{IP}(B) \sin \beta - M_{a'}(B) \cos \beta \quad (2b)$$

where M_{IP} ($M_{a'}$ and M_a) are the limiting values for $\beta = 90^\circ$ (0°) and defined to be positive and $M_a > M_{a'}$. This leads to an SMR Eq. (1)

$$\begin{aligned} \text{SMR}(B, \beta)/\rho_1 = & 1 - M_{IP}^2(B) \sin^2 \beta \\ & - \frac{1}{2}(M_a^2(B) + M_{a'}^2(B)) \cos^2 \beta \\ & - M_{IP}(M_a(B) - M_{a'}(B)) \sin \beta \cos \beta \end{aligned} \quad (3)$$

and $\text{SMR}(B, 0^\circ) = \rho_1 [1 - M_{IP}^2(B)]$ and $\text{SMR}(B, 90^\circ) = \rho_1 [1 - \frac{1}{2}(M_a^2(B) + M_{a'}^2(B))]$.

We estimate the ratio of the canting by an out-of-plane magnetic field relative to that of an in-plane magnetic field, $\sqrt{M_a^2 + M_{a'}^2}/2M_{IP}$, by fitting the observed SMR to Eq. (3) for $\rho_0 = 2060 \Omega$ and $\rho_1 = 2 \Omega$ as a function of magnetic field strength, see Fig. 4b). We arrive at ratios up to 0.6, which is much larger than expected considering the high exchange and anisotropy energy cost compared to the Zeeman energy gain. We note that the possibility of canting with a magnetic field parallel to the Néel vector has been discussed in the context of observations of off-diagonal elements in the magnetic susceptibility matrix [29].

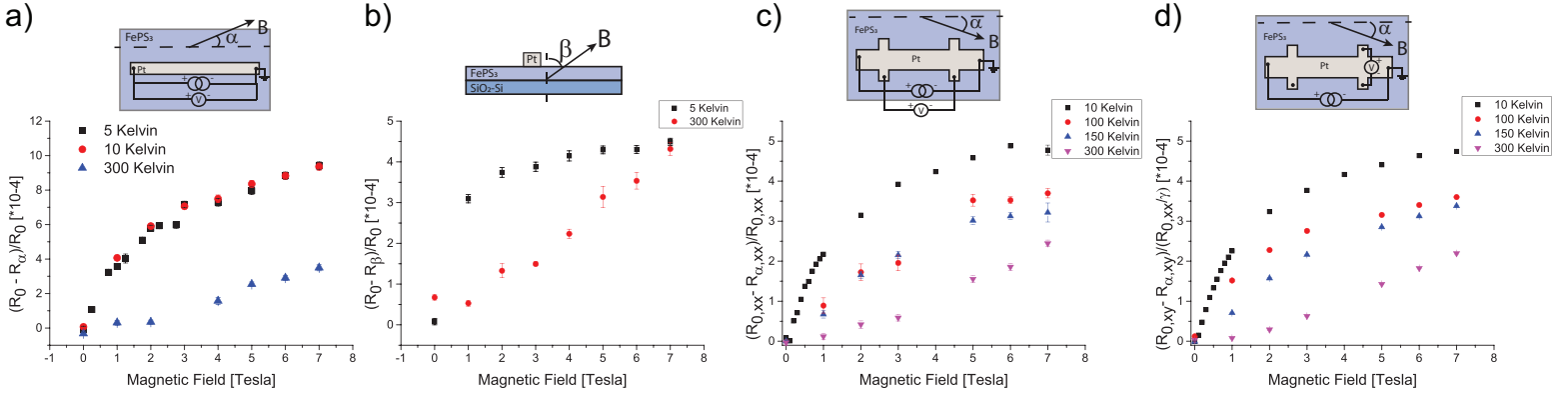


FIG. 5. Magnetic field dependent SMR amplitudes for an a) in-plane and b) out-of-plane rotation of the magnetic field at temperatures indicated in the inset. The magnetic field dependent longitudinal and transverse SMR amplitudes for various temperatures are shown in c) and d). $\gamma = 1.6$ is the geometric conversion factor which is the ratio between the length and the width of the Hall bar which is taken into account in order to compare the change in relative longitudinal resistance to the transverse results.

Fig. 5 displays the longitudinal and transverse SMR as a function of magnetic field strengths and directions for selected temperatures. The magnetization of bulk FePS₃ increases linearly with magnetic field strength [20], which according to Eq. (1), should result in a quadratic increase of the SMR amplitude. The observed linear increase with field is therefore an indication for different bulk and surface magnetizations.

Above the Néel temperature, SMR still exists but the difference between the α and β angular scans disappears in Fig. 4, therefore the effect of canting into the crystallographic **a** direction for an out-of-plane magnetic field disappears above T_N . The SMR amplitude decreases with increasing temperature by thermal fluctuations. Moreover, the second harmonic signal at room temperature is vanishingly small in spite of the finite SMR. This points to a very short magnon diffusion length or absence of long range order, since the bulk contribution dominates the spin Seebeck effect [30].

During finalization of this manuscript, Wu *et al.* posted an SMR study on the vdW antiferromagnet CrPS₄ [31]. This material has a very different spin configuration and small magnetic anisotropy. Its spin-flop transition at weak magnetic fields prohibits the canting we report here.

In conclusion, we succeeded in observing a strong SMR in exfoliated thin films of the perpendicular antiferromagnetic van der Waals material FePS₃ with Pt contacts. Below the Néel temperature, the SMR is very anisotropic at least up to field strengths of 7 T. The difference between the SMR and the field-induced magnetization of the bulk crystals is caused by a difference in the magnetization of the uppermost layer that should be indicative of the SMR in the monolayer limit. We observe a surprisingly large collective canting of the spins in the crystallographic **a** direction by an out-of-plane magnetic field. In the param-

agnetic regime the SMR signal of the field-induced magnetization loses the easy-plane anisotropy observed in the antiferromagnetic phase.

Our results reveal an unexpectedly complex field dependence of the magnetization of a representative van der Waals antiferromagnet. The SMR does not mirror the bulk magnetization because it senses only the uppermost monolayer and we do not expect that results change much in the monolayer limit. The technique can be used in principle for all van der Waals magnets onto which Pt films can be deposited.

We acknowledge the technical support from J. G. Holstein, H. Adema T. Schouten and H. de Vries. We acknowledge the financial support of the Zernike Institute for Advanced Materials. This project has been supported by the NWO Spinoza prize awarded to Prof. B. J. van Wees by the NWO. GB acknowledges funding by JSPS Kakenhi grant # 19H00645.

* e-mail: F.Feringa@rug.nl

† e-mail: B.J.van.Wees@rug.nl

- [1] V. Franco and B. Dodrill, *Magnetic Measurement Techniques for Materials Characterization* (2021).
- [2] K. S. Burch, D. Mandrus, and J. G. Park, *Nature* **563**, 47 (2018).
- [3] M. Gibertini, M. Koperski, A. F. Morpurgo, and K. S. Novoselov, *Nature Nanotechnology* **14**, 408 (2019).
- [4] H. Nakayama, M. Althammer, Y. T. Chen, K. Uchida, Y. Kajiwara, D. Kikuchi, T. Ohtani, S. Geprägs, M. Opel, S. Takahashi, R. Gross, G. E. Bauer, S. T. Goennenwein, and E. Saitoh, *Physical Review Letters* **110**, 1 (2013).
- [5] Y.-T. Chen, S. Takahashi, H. Nakayama, M. Althammer,

- S. T. B. Goennenwein, E. Saitoh, and G. E. W. Bauer, *Physical Review B* **87**, 144411 (2013).
- [6] N. Vlietstra, J. Shan, V. Castel, J. Ben Youssef, G. E. Bauer, and B. J. Van Wees, *Applied Physics Letters* **103**, 1 (2013).
- [7] N. Vlietstra, J. Shan, V. Castel, B. J. Van Wees, and J. Ben Youssef, *Physical Review B - Condensed Matter and Materials Physics* **87**, 1 (2013).
- [8] G. R. Hoogeboom, A. Aqeel, T. Kuschel, T. T. Palstra, and B. J. Van Wees, *Applied Physics Letters* **111**, 10.1063/1.4997588 (2017).
- [9] J. Fischer, O. Gomonay, R. Schlitz, K. Ganzhorn, N. Vlietstra, M. Althammer, H. Huebl, M. Opel, R. Gross, S. T. Goennenwein, and S. Geprägs, *Physical Review B* **97**, 1 (2018).
- [10] A. Aqeel, N. Vlietstra, J. A. Heuver, G. E. Bauer, B. Noheda, B. J. Van Wees, and T. T. Palstra, *Physical Review B - Condensed Matter and Materials Physics* **92**, 1 (2015).
- [11] M. Lammel, R. Schlitz, K. Geishendorf, D. Makarov, T. Kosub, S. Fabretti, H. Reichlova, R. Huebner, K. Nielsch, A. Thomas, and S. T. Goennenwein, *Applied Physics Letters* **114**, 10.1063/1.5090098 (2019).
- [12] R. Schlitz, T. Kosub, A. Thomas, S. Fabretti, K. Nielsch, D. Makarov, and S. T. Goennenwein, *Applied Physics Letters* **112**, 10.1063/1.5019934 (2018).
- [13] V. Eswara Phanindra, A. Das, J. J. L. van Rijn, S. Chen, B. J. van Wees, and T. Banerjee, (2022), [arXiv:2201.08685](https://arxiv.org/abs/2201.08685).
- [14] K. Oyanagi, J. M. Gomez-Perez, X. P. Zhang, T. Kikkawa, Y. Chen, E. Sagasta, A. Chuvilin, L. E. Hueso, V. N. Golovach, F. S. Bergeret, F. Casanova, and E. Saitoh, *Physical Review B* **104**, 1 (2021).
- [15] R. Lebrun, A. Ross, O. Gomonay, S. A. Bender, L. Baldrati, F. Kronast, A. Qaiumzadeh, J. Sinova, A. Brataas, R. A. Duine, and M. Kläui, *Communications Physics* **2**, 1 (2019).
- [16] G. R. Hoogeboom, T. Kuschel, G. E. Bauer, M. V. Mostovoy, A. V. Kimel, and B. J. Van Wees, *Physical Review B* **103**, 134406 (2021).
- [17] S. Damerio, A. A. Kaverzin, V. Ocelík, G. R. Hoogeboom, B. J. van Wees, and B. Noheda, *Advanced Electronic Materials* **2100963**, 2100963 (2021).
- [18] K. Momma and F. Izumi, *Journal of Applied Crystallography* **44**, 1272 (2011).
- [19] S. Geprägs, M. Opel, J. Fischer, O. Gomonay, P. Schwenke, M. Althammer, H. Huebl, and R. Gross, *Journal of Applied Physics* **127**, 10.1063/5.0009529 (2020).
- [20] See Supplemental Material Section S6 at [URL will be inserted by publisher] for more details on the magnetization and magnetic susceptibility measurements. ().
- [21] G. Ouvrard, R. Brec, and J. Rouxel, *Materials Research Bulletin* **20**, 1181 (1985).
- [22] J. U. Lee, S. Lee, J. H. Ryoo, S. Kang, T. Y. Kim, P. Kim, C. H. Park, J. G. Park, and H. Cheong, *Nano Letters* **16**, 7433 (2016).
- [23] P. a. Joy and S. Vasudevan, *Physical Review B* **46**, 5425 (1992).
- [24] F. Wang, T. A. Shifa, P. Yu, P. He, Y. Liu, F. Wang, Z. Wang, X. Zhan, X. Lou, F. Xia, and J. He, *Advanced Functional Materials* **28**, 1 (2018).
- [25] See Supplemental Material Section S3 at [URL will be inserted by publisher] for more details. ().
- [26] K. S. Novoselov, D. Jiang, F. Schedin, T. J. Booth, V. V. Khotkevich, S. V. Morozov, and A. K. Geim, *Proceedings of the National Academy of Sciences of the United States of America* **102**, 10451 (2005).
- [27] *HQ Graphene*.
- [28] A. R. Wildes, D. Lançon, M. K. Chan, F. Weickert, N. Harrison, V. Simonet, M. E. Zhitomirsky, M. V. Gvozdkova, T. Ziman, and H. M. Rønnow, *Physical Review B* **101**, 24415 (2020).
- [29] M. Nauman, D. H. Kiem, S. Lee, S. Son, J. G. Park, W. Kang, M. J. Han, and Y. Jo, *2D Materials* **8**, 10.1088/2053-1583/abeed3 (2021).
- [30] See Supplemental Material Section S2 at [URL will be inserted by publisher] for more details on the second harmonic measurements. ().
- [31] R. Wu, A. Ross, S. Ding, Y. Peng, F. He, Y. Ren, R. Lebrun, Y. Wu, Z. Wang, J. Yang, A. Brataas, and M. Kläui, (2021), [arXiv:2112.07306](https://arxiv.org/abs/2112.07306).